energy&fuels

Article

pubs.acs.org/EF

Optical Properties and Radiation-Enhanced Evaporation of Nanofluid Fuels Containing Carbon-Based Nanostructures

Yanan Gan and Li Qiao*

School of Aeronautics and Astronautics, Purdue University, West Lafayette, Indiana 47907, United States

ABSTRACT: The present paper experimentally determined the evaporation characteristics of nanofluid fuels with stable suspension of carbon-based nanostructures under radiation absorption in the ultraviolet−visible range. The results show that the evaporation rates of the ethanol-based nanofluids containing multiwalled carbon nanotubes (MWCNTs) or carbon nanoparticles (CNPs) are both higher than the evaporation rate of pure ethanol. Additionally, ethanol fuel with the addition of MWCNTs has a higher droplet temperature and a higher evaporation rate than the one with the addition of CNPs or aluminum (Al). To determine the optical properties of various nanofluids, which can help to explain the observed evaporation behavior, we measured the transmission spectrum for each nanofluid, and the extinction coefficient was determined accordingly. The optical properties were also modeled using Rayleigh approximation. The importance of radiation absorption and scattering by the suspended nanostructures was identified for various nanofluids. The results show that MWCNTs are more effective than Al and CNPs for radiation absorption in nanofluid because less energy is scattered away.

1. INTRODUCTION

Nanofluids are liquids with stable suspensions of nanoscale (typically 1−100 nm) materials. The nanomaterials can be metals, oxides, carbides, nitrides, or carbon-based nanostructures that can be of various shapes, such as sphere, rod, fiber, disk, and tube. Many studies have reported that nanofluids exhibit significantly enhanced thermal conductivity.[1−4] Because of this unique property, they have great potential to be used in different kinds of energy and thermal systems as an advanced heat-transfer fluid, e.g., advanced cooling of electronics systems and microelectromechanical systems (MEMS).[1] Several theories have been proposed to explain the fundamental mechanisms for enhanced thermal conductivity.[1] One, for example, suggests that it is because of the nanoconvection caused by the random Brownian motion of nanoparticles.[5,6] Another proposes that the layered structure is acting as a thermal bridge between a solid nanoparticle and a bulk liquid.[7,8] Others believe that aggregation of nanoparticles plays an important role for heat conductivity enhancement.[9−11] Despite many studies, our understanding of the thermal conductivity of nanofluids is still incomplete.

The present paper is based on a new concept, nanofluid-type fuels, which have generated much interest in the combustion and propulsion communities. Nanoscale materials (mainly energetic nanomaterials and nanocatalysts) were suggested as additives for mixing with traditional liquid fuels in a proper way to enhance ignition and combustion. Previous studies have shown elevated performance by nanofluid fuels that contain the addition of energetic nanomaterials, such as aluminum and boron, and nanocatalysts, such as cerium oxide. These improvements included higher energy release,[12] shortened ignition delay,[13] increased burning rate,[14,15] increased ignition probability,[16] and enhanced catalytic effects.[17,18] However, the applications of nanofluid fuels may be limited by issues such as particle aggregation and potential emissions of metal oxide particles.

Most recently, carbon-based nanomaterials have also been suggested as fuel additives because of their unique thermal and optical properties. Sabourin et al.[19] discovered that the addition of only 1% (by mass) functionalized graphene sheets to monopropellant nitromethane can significantly enhance the burning rate and also lower the ignition temperature. Finigan et al.[20] recently found that carbon nanotubes (CNTs) could be used for distributed photo-ignition of fuel/oxidizer mixtures, similar to the flash ignition of Al nanoparticles.[21] Furthermore, the authors observed flame acceleration and deflagration−detonation transition as a result of the distributed ignition.

Radiative heat transfer plays an important role in combustion.[22] For example, in diesel engines, it contributes 20−35% of the total heat transfer,[23] mostly coming from high-temperature soot particles formed during combustion processes. However, knowledge on the radiative heat-transfer properties of nanofluid fuels does not exist. A fundamental understanding of the optical properties of nanofluid fuels is important for their application in combustion and propulsion systems. Radiative heat transfer in a multiphase system, such as nanofluids, is highly complex. The base fluid and particles can both be an absorber with different absorption abilities; thus, it is possible that there is a temperature gradient between the particles and the base fluid. Moreover, scattering over the particle surface will take place, and the mode of scattering depends upon several factors, such as particle size (Rayleigh or Mie scattering), geometry, and volume fraction (dependent or independent; multiple or single scattering). In the latter, the interactions of the scattered radiation waves from neighboring particles and the secondary scattering over neighboring particles must be considered.

Received: March 22, 2012
Revised: May 25, 2012
Published: May 29, 2012

dx.doi.org/10.1021/ef300493m | *Energy Fuels* 2012, 26, 4224−4230

In our previous study,[24] we have investigated the radiative properties of various nanofluid fuels containing Al and Al_2O_3, as well as their effects on the droplet evaporation rate when exposed to radiation. The results show that the nanofluid with Al nanoparticles has a higher droplet evaporation rate than the one with Al_2O_3 nanoparticles. However, at high particle-loading rates, such enhancement was mitigated by the increasing aggregation of nanoparticles, which tends to inhibit diffusion and suppress evaporation.

The present paper examines the radiative properties of nanofluid fuels with suspensions of carbon nanostructures, including carbon nanoparticles (CNPs) and CNTs. Because of their unique structures and unusual mechanical and electric properties, CNTs have been widely studied as applications in material, electrical, and biomedical sciences.[25,26] They also have unique thermal properties; e.g., CNTs are reported to have unusually high thermal conductivity compared to the bulk material—graphene monolayer.[27,28] Intensive investigation has been conducted into the thermal conductivity of nanofluids with CNTs.[29−33]

However, the optical and radiative properties of nanofluids with carbon-based nanostructures, as well as their impact on droplet evaporation and combustion, have not been studied. Thus, this paper first reported the evaporation behavior of nanofluid droplets with suspensions of CNTs and CNPs under radiation absorption. Then, the transmission spectra of these nanofluids were measured, and the extinction coefficients compared to theoretical results predicted by Rayleigh approximation were determined. The relative importance of radiation absorption and scattering by the nanoparticles was discussed with regard to different nanofluids. Lastly, the results were used to explain the observed evaporation behavior.

2. EXPERIMENTAL SECTION

The preparation methods for nanofluid fuels are essentially the same as in our previous studies.[34,35] Briefly, the physical method (using ultrasonic waves) and the chemical method (using a surfactant or polymer) were both used to disperse the nanostructures homogenously in the base fuel and to minimize agglomeration. The duration and power levels of the ultrasonic treatment were carefully controlled to prevent damage to the structure of CNTs. Ethanol was chosen as the base fuel; we have shown in a previous study that good suspension quality of nanoparticles in ethanol can be achieved even without the use of a surfactant.[34] Three types of carbon-based nanostructures were studied here as fuel additives, including CNPs and single-walled and multiwalled carbon nanotubes (SWCNTs and MWCNTs).

Figure 1 shows transmission electron microscopy (TEM) images of the samples studied. All were purchased from Nanostructured and Amorphous Materials, Inc., with no further treatments. The TEM image of CNPs with a mean diameter of 6 nm is shown in Figure 1a. The CNPs can be seen to have a quite uniform size. However, they tend to agglomerate. Figure 1b shows the TEM image of the SWCNTs. The diameter of the SWCNTs is 1−2 nm, and the length is 5−30 μm. Because of the large aspect ratio, the SWCNTs tend to entangle with one another and form network structures. Single and isolated SWCNTs are fewer. The characteristic size of the network structures is about 10 μm. The TEM image of the dispersible MWCNTs is shown in Figure 1c. The dispersible MWCNTs are coated with selected polymers in solid powder form. The polymers functionalized the surface of MWCNTs to be hydrophilic; thus, the stability of MWCNTs dispersed in polar fuels (such as ethanol) can be significantly enhanced. In comparison to the SWCNTs in Figure 1b, the MWCNTs in Figure 1c are more separated and show much fewer network structures because of entanglement. Also, the length of the MWCNTs is about 100 nm, significantly shorter than that of the SWCNTs.

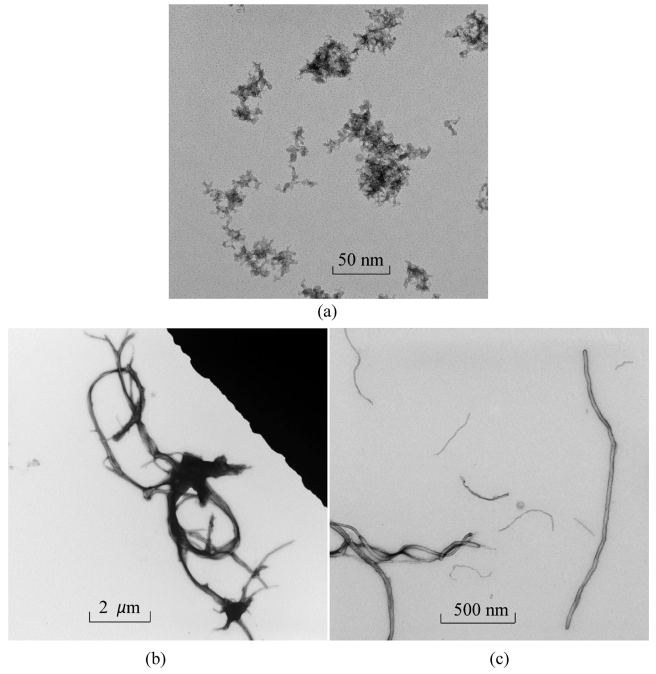

Figure 1. TEM images of (a) CNPs (6 nm), (b) SWCNTs (diameter, 1−2 nm; length, 5−30 μm), and (c) dispersible MWCNTs (diameter, 20 nm; length, 1−5 μm). Images were taken by FEI/Philips CM-100 TEM.

The suspension quality of the nanofluid fuels was compared. For the purpose of comparison, the loading rate of all nanostructures was kept at 0.1 wt % with no surfactant being added. Suspension quality was evaluated on the basis of the time that it takes for all particles to settle at the bottom of the test tube after sonication. SWCNTs were found to have the worst suspension quality; all of the SWCNTs settled in about 5 min. It was difficult to use an ultrasonic bath to break the network structures and to separate the SWCNTs from one another. Immediately after sonication, visible agglomerates were formed. Because of the quick and strong agglomeration of SWCNTs that a table suspension cannot maintain, we did not study fuels with the addition of SWCNTs. Instead, dispersible MWCNTs were used, which have much better suspension quality; good suspension was well-maintained for at least 4 weeks. The suspension quality of ethanol with CNPs is good; it can maintain stable for more than 24 h. This is comparable to ethanol with Al nanoparticles, which we have previously studied.

The droplet evaporation experiment was described in detail in our previous study [24]. Here we will only briefly describe the experimental setup. A mercury lamp was used as a radiation source with adjustable light intensity, for which most of the radiation energy lies in the UV and visible range. The radiation from the lamp was collimated to a beam size of 5mm in diameter. The evaporation process of a suspended nanofluid droplet, which was placed in a closed chamber with optical access, was recorded using a high-speed camera. Images were processed by a self-developed MATLAB code to derive the droplet evaporation rate. A type K thermocouple with a thickness of 76 μm was used to suspend the nanofluid droplet for all the tests. The initial size of the suspended droplets was around 1.2 mm. Thus the nanofluid droplet size and temperature history can be monitored simultaneously. For each test condition, the experiment was repeated at least three times, and an averaged evaporation rate was obtained with an error bar to indicate the standard deviation.

3. RESULTS AND DISCUSSION

3.1. Evaporation of Nanofluid Droplets under Radiation. First, the evaporation rate of pure ethanol droplets under various radiation levels was examined as a baseline for

dx.doi.org/10.1021/ef300493m | Energy Fuels 2012, 26, 4224−4230

studying the effect of the addition of carbon-based nanostructures. As indicated in Figure 2, the evaporation rate of the ethanol droplet increases with the power level of the mercury lamp. An increase of 13.4% was observed when the power level was increased to 175 W, from 75 W. This indicates that part of the radiation energy was absorbed by the ethanol droplet, which increases the evaporation rate.

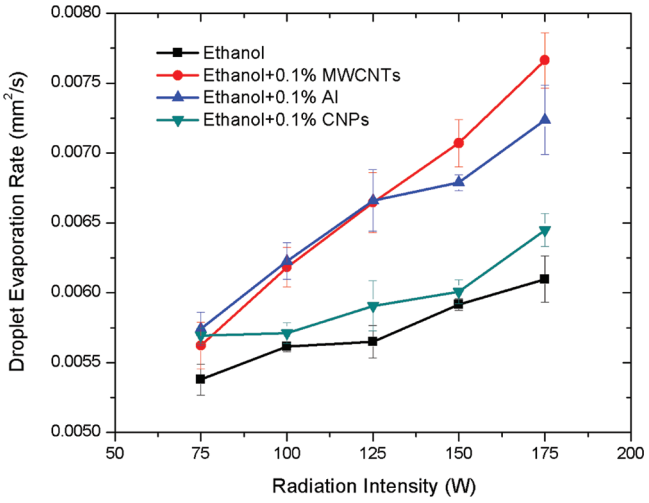

Figure 2. Droplet evaporation rate of pure ethanol and nanofluids with the addition of Al particles, CNPs, and dispersible MWCNTs at different radiation levels.

We then investigated the evaporation rates of ethanol with MWCNTs and CNPs. Note that the loading rate was kept at 0.1 wt % in all instances. The results show that the evaporation rate of all nanofluids increases when the power level of the mercury lamp increases. The evaporation rates of all nanofluids are higher than those of pure ethanol at all radiation levels. However, the level of droplet evaporation rate enhancement differs. The enhancement was most significant for the nanofluid with MWCNTs, an increase of 25.6% at 175 W compared to the evaporation rate of pure ethanol. For a purpose of comparison, Figure 2 also shows the evaporation rates of ethanol with the addition of Al particles (the average size is 80 nm, and the concentration is the same at 0.1 wt %). The enhancement for the nanofluid with Al nanoparticles was weaker than with MWCNTs, an increase of 18.7% at 175 W. Lastly, the evaporation rates of the nanofluid with CNPs are only slightly higher than that of pure ethanol, a slight increase of 5.7% at 175 W.

When the droplets are exposed to radiation, part of the radiation energy will be reflected away on the droplet surface and the rest will be refracted into the droplet. Part of the refracted radiation will be either absorbed or scattered by the nanofluid, and the rest will be transmitted through the droplet. Radiation absorption by both the base fuel and the suspended nanostructures can enhance droplet evaporation. Because the base fuel is the same for all situations discussed above, the different evaporation enhancement is most likely because of the various radiation absorption abilities of the nanostructures.

3.2. Droplet Temperature History. To further understand the radiative heat transfer inside an evaporating nanofluid droplet, we measured the droplet temperature history, which has a direct correlation with the evaporation rate. Here, we used a thermocouple to suspend the nanofluid droplet and, simultaneously, to measure the droplet temperature.

Figure 3 shows the temperature histories of evaporating nanofluid droplets containing 0.1 wt % SWCNTs, MWCNTs, and CNPs and when the power of the mercury lamp was set at 175 W. The temperature profiles of these nanofluid droplets share some similarities. Before t = 10 s, when the radiation source is blocked from the droplet, the temperatures of all droplets are essentially the same (about 10.5 °C). Immediately after the droplet is exposed to radiation from the mercury lamp, the droplet temperature undergoes a steep rise. After this transition stage, steady-state evaporation has been established and the droplet temperature approaches a constant value.

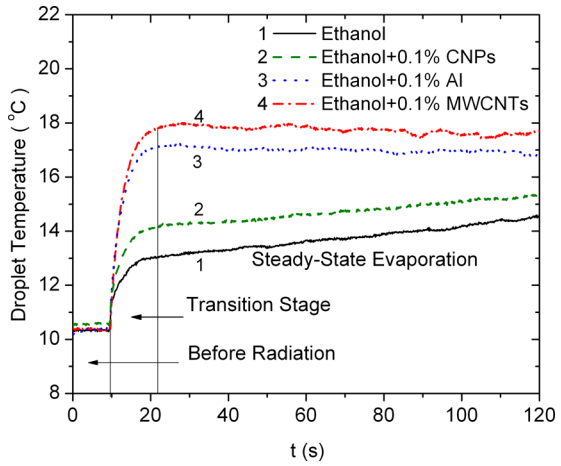

Figure 3. Droplet temperature history of pure ethanol and nanofluids with the addition of Al particles, CNPs, and dispersible MWCNTs.

Despite these similarities, there are major differences. For the transition stage, the nanofluids with MWCNTs and Al nanoparticles have a steeper increase of the droplet temperature than with CNPs and pure ethanol. After the transition stage, a higher droplet temperature was observed for the nanofluids with MWCNTs (18 °C) and Al nanoparticles (17 °C) than with CNPs (15 °C) or pure ethanol (14.5 °C). These results indicate that more radiation energy may be absorbed and will dissipate in the nanofluids with MWCNTs and Al nanoparticles, resulting in higher droplet temperatures and, consequently, higher evaporation rates.

3.3. Transmission Spectrum. To quantitatively determine the wavelength-dependent radiation absorption and scattering, we measured the transmission spectrum of the nanofluids in the UV−vis range, which corresponds to the spectrum of the mercury lamp that was used as a radiation source. For the transmission spectrum measurement, the nanofluid was placed in a fused quartz cuvette with a thickness of 1 mm. A UV−vis spectrometer was used to detect the transmitted light and to calculate the corresponding transmission spectrum.

Figure 4 shows the transmission spectra of pure ethanol, ethanol with Al nanoparticles, CNPs, and MWCNTs. Pure ethanol is almost transparent to radiation in the visible range (>360 nm), with a transmittance of more than 90%. A quick drop of transmittance was observed in the UV range, which indicates a strong absorption of radiation energy by ethanol in this range. In comparison to pure ethanol, nanofluids with Al nanoparticles, CNPs, and MWCNTs have a much lower transmittance. Among them, ethanol with Al nanoparticles

dx.doi.org/10.1021/ef300493m | Energy Fuels 2012, 26, 4224−4230

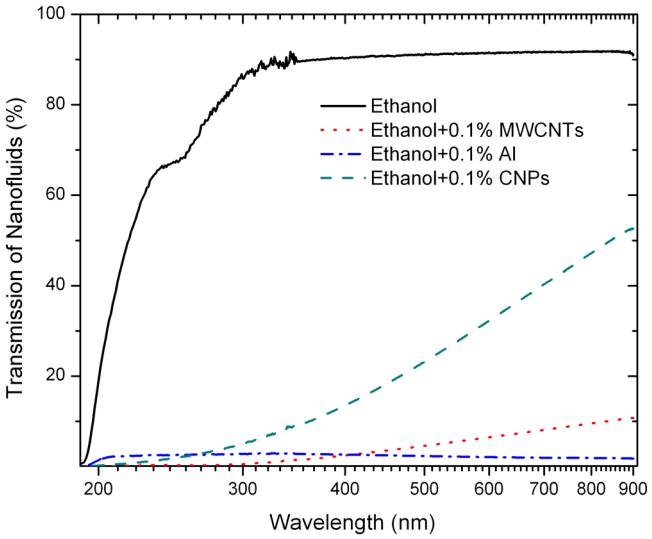

Figure 4. Transmission spectrum of pure ethanol and nanofluids with the addition of Al particles, CNPs, and dispersible MWCNTs.

shows the lowest transmission; only 2% of the light was transmitted over most of the spectrum. The nanofluid with MWCNTs has lower transmission in the UV range but higher transmission in the visible range. Because most of the radiation energy from the mercury lamp lies in the visible range, the nanofluid with MWCNTs has a higher overall transmission than that with Al nanoparticles. The nanofluid with CNPs has a higher transmission than the other two nanofluids. Lastly, in comparison to the spectrum of pure ethanol, we observed no steep drop of transmittance for the nanofluids when the radiation is shifted from the visible range to the UV range.

On the basis of the measured transmission spectrum, we calculated the extinction coefficient of the nanofluids using the Lambert–Beer law. The thickness of the tested nanofluid sample is 1 mm in the present experiment. The results are shown in Figure 5. The extinction coefficient of ethanol is very low, only 1 cm^{-1} in the visible range. For the nanofluids with

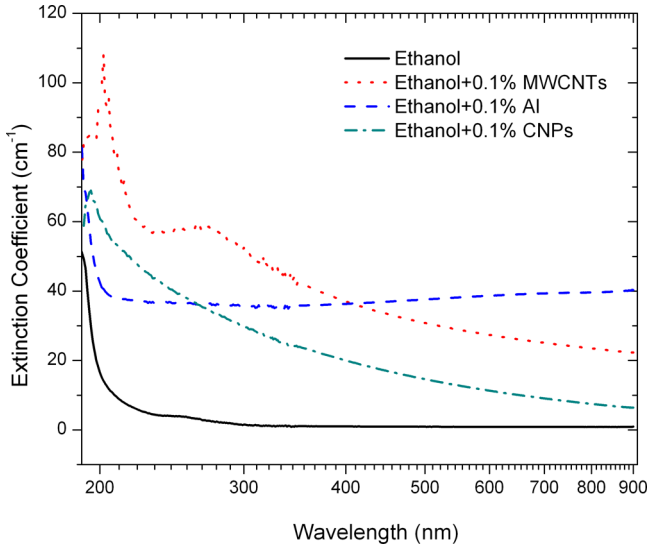

Figure 5. Measured extinction coefficient of pure ethanol and nanofluids with the addition of Al particles, CNPs, and dispersible MWCNTs.

carbon nanostructures (MWCNTs and CNPs), the extinction coefficient decreases with an increasing wavelength. The nanofluid with MWCNTs has a higher extinction coefficient than with CNPs. For the nanofluid with Al nanoparticles, a stable extinction coefficient of about 40 cm^{-1} was observed for most of the wavelength range.

We noticed an interesting phenomenon when comparing the transmission spectrum, droplet evaporation rates, and temperature histories of these nanofluids. The nanofluid with Al nanoparticles has the lowest transmission, which may indicate the strongest radiation absorption; thus, it is expected to have the highest droplet temperature and evaporation rate. However, as shown in Figures 2 and 3, the nanofluid with Al nanoparticles has a lower droplet temperature and evaporation rate than the nanofluid with MWCNTs.

It is well-known that light extinction is due to both absorption and scattering. The absorbed radiation energy, especially by particles, will be used to heat the droplet and, thus, contribute to the increase of the droplet temperature and evaporation rate. The scattered energy, however, will be largely dissipated into the environment and, thus, will not contribute to the heat transfer to the droplet. Thus, our speculation is that more radiation energy is scattered away by Al nanoparticles than by MWCNTs. Motivated by this, in the following section, we will theoretically model the radiation properties of the nanofluids and quantitatively determine the relative importance of absorption and scattering.

3.4. Modeling of the Optical Properties of the Nanofluid Fuels. When thermal radiation interacts with a medium containing particles, the radiative intensity will be changed because of absorption by and scattering from the particles.[36] Our goal here is to understand radiative heat-transfer mechanisms in the nanofluids containing carbon-based nanostructures, especially the interaction between absorption and scattering, resulting from the presence of the nanostructures. Nanofluids are two-phase systems; the optical properties of the solid and liquid phases will be modeled separately as a first step. The results will then be combined to determine the radiation properties of the nanofluids.

We will first discuss radiation absorption and scattering from nanoparticles. Four parameters (interparticle distance, particle shape, particle material, and particle size) fundamentally determine the amount of radiation energy that is absorbed or scattered.[36] In the present modeling, the particle size will be characterized by size parameter α, which is defined as $\alpha = \pi D/\lambda$, where D is the particle diameter and λ is the wavelength. The effect of particle material is reflected by the index of refraction and absorption of the material. The estimated interparticle distance based on particle size and volume fraction determines the scattering pattern, e.g., independent or multiple and dependent scattering. For simplicity, the shapes of all of the nanostructures are assumed to be spherical, including CNTs, which have large aspect ratios. It is reported that CNTs exhibit strong nonlinear optical properties because of their unique geometry, and this will also result in optical limiting behaviors.[37−40] The nonlinear optical properties and the related optical limiting behaviors of CNTs are quite complicated and may deserve a separate study.[41] Because of this, here we have assumed a spherical geometry for CNT. This assumption will certainly bring in inaccuracy when modeling light scattering and absorption by them. Nevertheless, our goal here is to understand the overall optical properties of nanofluid fuels. The modeling, although simplified for CNTs, can provide

dx.doi.org/10.1021/ef300493m | Energy Fuels 2012, 26, 4224−4230

a qualitative understanding of the dominant factors that are responsible for the enhancement of the droplet evaporation rate.

The scattering pattern, whether it is independent, multiple, or dependent, is largely affected by the particle concentration or, in other words, interparticle distance. For multiple scattering, the scattered wave from one particle becomes the incident on another and is then scattered again. Dependent scattering happens when the scattered waves from neighboring particles interfere with one another. For the nanoparticles and CNTs studied in this paper, their characteristic size is in the range of 6−80 nm. When the nanoparticles are properly suspended in the base fluid and assuming that they are evenly distributed, the interparticle distance can be estimated on the basis of the particle size and volume fraction (f_v). Figure 6

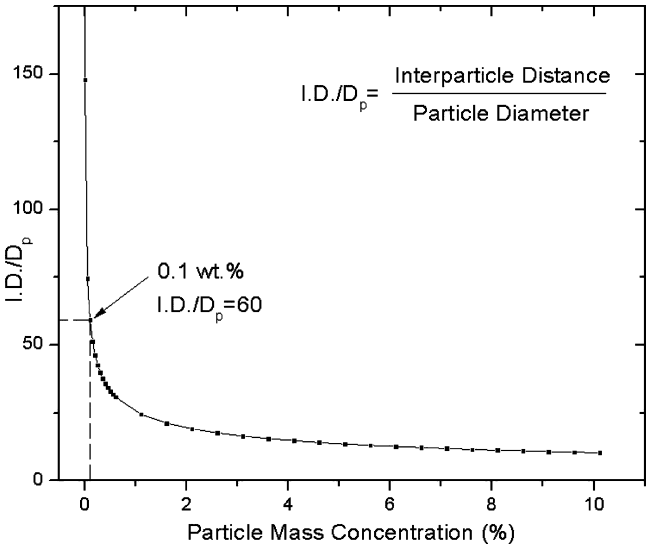

Figure 6. Nanoparticle spacing ratio at different particle mass concentrations for nanofluid.

shows the particle spacing ratio as a function of the mass concentration for the nanofluids. The spacing ratio is defined as the ratio of the interparticle distance (ID) to particle size, and it was calculated on the basis of the following equation:[42]

$$\frac{\mathrm{ID}}{D} = 2.77 f_v^{-0.381} \tag{1}$$

Figure 6 shows that, for the dilute nanofluids (0.1% by mass) studied in this paper, the spacing ratio is about 60. For the scattering over spherical particles, independent scattering will happen if the following criteria can be met:[22]

$$\mathrm{ID} + 0.1D > \lambda/2 \tag{2}$$

With these criteria, we may conclude that the effect of multiple and dependent scattering can be neglected for the present dilute nanofluids (0.1% by mass). Thus, scattering from particles was assumed to be independent and single scattering. The scattering from the solid phase will be a sum of scattering from all particles. This conclusion is also consistent with the classic treatment of the scattering pattern for particulate systems developed by Tien.[43] Figure 7 shows that Tien divided the scattering map into several regimes for various particulate systems. As we can see, the particle system of nanofluids with 0.1 wt % particles lies in the independent scattering zone.

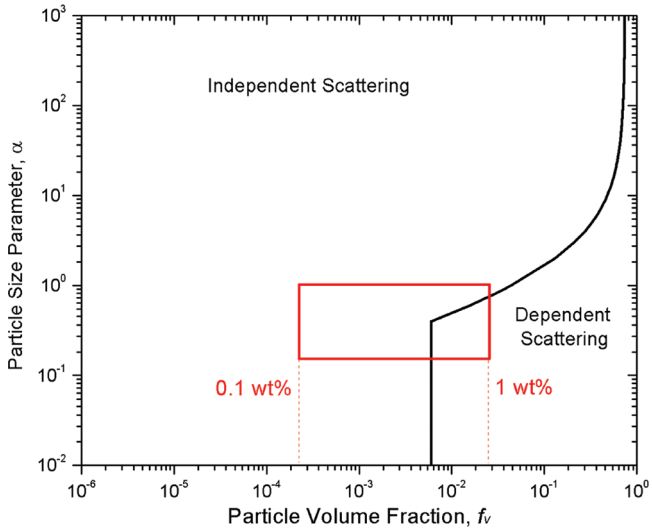

Figure 7. Dependent and independent scattering regime map for different particulate systems (modified on the basis of ref 39).

The fundamental absorption and scattering characteristics of a single particle can be obtained by solving the electromagnetic field equations.[43] Because the characteristic particle sizes are in the range of 6−80 nm for the present nanofluids, which are much smaller than the wavelength (190−900 nm) of radiation, the scattering is mainly Rayleigh scattering. Because of the small size parameter ($\alpha < 1$), the solution for Rayleigh scattering can be simplified using the Rayleigh approximation equations.[36] The equations to calculate the scattering (Q_{scat}), absorption (Q_{abs}), and extinction (Q_{ext}) efficiencies are as follows:[36]

$$Q_{scat} = \frac{8}{3}\alpha^4 Re\left[\left(\frac{m^2-1}{m^2+2}\right)^2\right] \tag{3}$$

$$Q_{abs} = 4\alpha\ \mathrm{Im}\left\{\frac{m^2-1}{m^2+2}\left[1 + \frac{\alpha^2}{15}\left(\frac{m^2-1}{m^2+2}\right)\frac{m^4+27m^2+38}{2m^2+3}\right]\right\} \tag{4}$$

$$Q_{ext} = Q_{scat} + Q_{abs} \tag{5}$$

where m is the relative complex refractive index of the nanofluid, defined as $m = n_p/n_f$, in which n_p and n_f are the complex refractive index of the nanoparticles and the base fluid, respectively. All relevant optical properties, including the index of refraction and absorption, were obtained from a handbook.[44] In particular, the optical properties of the bulk material graphite were used for MWCNTs, and the properties of the bulk material diamonds were used for CNPs because CNPs are made from synthetic diamonds. The optical properties of the MWCNTs are quite wavelength-dependent, whereas the optical properties of CNPs are constant over most of the wavelength range. On the basis of the extinction efficiency of nanoparticles, we can calculate the extinction coefficient σ_p using the following equation:[42]

$$\sigma_p = \frac{3\pi}{2}\frac{f_v Q_{ext}}{D} \tag{6}$$

dx.doi.org/10.1021/ef300493m | Energy Fuels 2012, 26, 4224−4230

Next, we will calculate the extinction coefficient of radiation energy by the base fluid. As seen from the transmission spectrum (Figure 4), ethanol is almost transparent in the visible range. However, it has very strong absorption in the UV range. Because there is no scattering from the base fluid, we need only to consider the absorption of radiation by the base fluid. The extinction coefficient σ_f can be calculated using the following equation:[42]

$$\sigma_f = \frac{4\pi k_f}{\lambda} \tag{7}$$

where k_f is the imaginary part of the complex refractive index of the base fluid.

Lastly, we can calculate the total extinction coefficient of the nanofluids by adding the extinction coefficient of the nanoparticles and the base fluid together.

$$\sigma = \sigma_f + \sigma_p = \frac{3\pi}{2}\frac{f_v Q_{ext}}{D} + \frac{4\pi k_f}{\lambda} \tag{8}$$

The theoretically predicted extinction coefficients of various nanofluids studied in this paper are shown in Figure 8. A

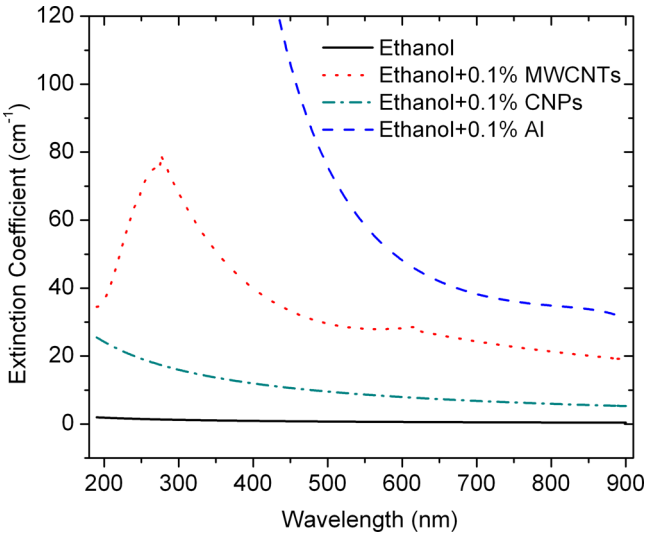

Figure 8. Calculated extinction coefficient of pure ethanol and nanofluids with the addition of Al particles, CNPs, and dispersible MWCNTs.

qualitative agreement, as compared to the measured values (Figure 5), was achieved for ethanol and the nanofluids with CNPs and MWCNTs in the visible range. However, disagreement in the UV range is significant. For the nanofluid with Al nanoparticles, significant disagreement was observed in both the visible and UV ranges. Especially in the UV range, the predicted coefficients are of one magnitude higher than the measured values. This is because the size parameter of Al nanoparticles is close to unity in the visible range and is larger than unity in the UV range, which means that the Rayleigh approximation is no longer valid and an alternative treatment should be used here. For particles with size parameters larger than the unit, the Mie scattering theory should be adopted to calculate the absorption and scattering.[45] This is the work planned in our future study.

We also compared the scattering (Q_{scat}) and absorption (Q_{abs}) efficiencies of the nanofluids with MWCNTs and Al nanoparticles, as shown in Figure 9. Figure 9a shows that the

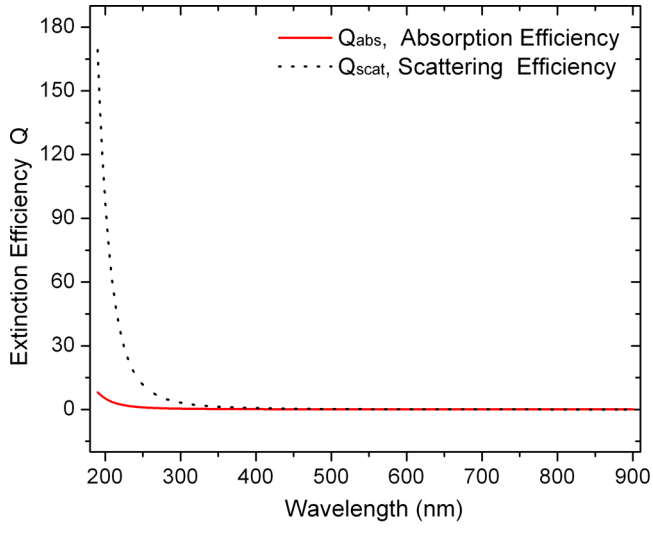

(a)

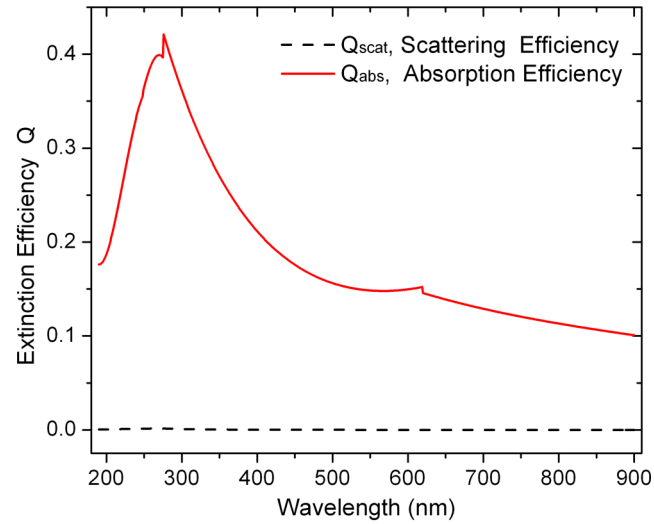

(b)

Figure 9. Calculated extinction efficiency of nanofluids with (a) Al nanoparticles and (b) MWCNTs.

scattering efficiency from Al nanoparticles is much higher than the absorption efficiency. However, for the MWCNTs in Figure 9b, the absorption efficiency is more significant than the scattering efficiency. This helps to explain the phenomenon that we observed in the previous section; that is, the nanofluid with Al nanoparticles has a lower droplet temperature and evaporation rate than the nanofluid with MWCNTs, although its transmittance is lower. This is because, even though the total extinction of light is higher for the nanofluid with Al nanoparticles, much of the radiation energy is indeed scattered away and, thus, will not contribute to the heat deposit within the nanofluid droplet. For the nanofluid with MWCNTs, however, most of the radiation energy will be absorbed by the MWCNTs and then dissipated within the droplet. As a result, the droplet temperature of the nanofluid with MWCNTs is higher and the droplet evaporation rate is significantly enhanced. Lastly, it is noted that particle aggregation was not considered in the modeling. Particle aggregation is a highly complex process, which will change particle size and morphology. Nevertheless, the present paper considered dilute nanofluids with a particle concentration of 0.1 wt %; thus, the

dx.doi.org/10.1021/ef300493m | Energy Fuels 2012, 26, 4224−4230

assumptions made in the modeling are reasonable as a first step toward understanding a very complex phenomenon.

4. CONCLUSION

The optical properties of and radiative heat transfer within several nanofluid fuels with a stable suspension of carbon-based nanostructures were investigated for the first time. The evaporation characteristics of these nanofluids were determined when exposed to radiation in the UV−vis range. The major conclusions are as follows: (1) The results reveal that the ethanol-based nanofluids with the addition of MWCNTs or CNPs both have a higher droplet evaporation rate than pure ethanol. Additionally, ethanol with MWCNTs can achieve a higher droplet temperature and, thus, a significantly increased droplet evaporation rate than those with CNPs or Al. (2) To quantitatively determine the wavelength-dependent radiation absorption and scattering, the transmission spectrum of these nanofluids was measured and the extinction coefficient was determined on the basis of the Lambert−Beer law. In comparison to pure ethanol, the nanofluids with Al nanoparticles, CNPs, and MWCNTs have a much lower transmittance. Among them, ethanol with Al nanoparticles shows the lowest transmission; only 2% of the light was transmitted over most of the spectrum. Additionally, the nanofluid with MWCNTs has a lower transmission in the UV range but a higher transmission in the visible range. (3) The optical properties of these nanofluids, including absorption, scattering, and extinction, were also theoretically modeled using the Rayleigh approximation. The results show that MWCNTs in nanofluid are more effective for radiation absorption in comparison to Al or CNPs because less energy is scattered away.

■ AUTHOR INFORMATION

Corresponding Author

*Telephone: 765-494-2040. E-mail: lqiao@purdue.edu.

Notes

The authors declare no competing financial interest.

■ ACKNOWLEDGMENTS

This work has been supported by the Army Research Office (ARO), with Dr. Ralph Anthenien as the technical monitor.

■ REFERENCES

(1) Choi, S. U. S. *J. Heat Transfer* **2009**, *131*, No. 033106.
(2) Yu, W. H.; et al. *Heat Transfer Eng.* **2008**, *29*, 432−460.
(3) Das, S. K.; Choi, S. U. S.; Patel, H. E. *Heat Transfer Eng.* **2006**, *27*, 3−19.
(4) Choi, S. U. S. *Proceedings of the International Mechanical Engineering Congress and Exhibition*; San Francisco, CA, Nov 12−17, 1995.
(5) Jang, S. P.; Choi, S. U. S. *Appl. Phys. Lett.* **2004**, *84*, 4316−4318.
(6) Prasher, R.; Bhattacharya, P.; Phelan, P. E. *Phys. Rev. Lett.* **2005**, *94*, No. 025901.
(7) Yu, W.; Choi, S. U. S. *J. Nanopart. Res.* **2003**, *5*, 167−171.
(8) Liang, Z.; Tsai, H.-L. *Phys. Rev. E: Stat. Phys., Plasmas, Fluids, Relat. Interdiscip. Top.* **2011**, *83*, No. 041602.
(9) Xuan, Y.; Li, Q.; Hu, W. *AIChE J.* **2003**, *49*, 1038−1043.
(10) Timofeeva, E. V.; et al. *Phys. Rev. E: Stat. Phys., Plasmas, Fluids, Relat. Interdiscip. Top.* **2007**, *76*, No. 061203.
(11) Wu, C.; et al. *Phys. Rev. E: Stat. Phys., Plasmas, Fluids, Relat. Interdiscip. Top.* **2010**, *81*, No. 011406.
(12) Jones, M.; et al. *Nanoscale Res. Lett.* **2011**, *6*, 1−12.
(13) Allen, C.; et al. *Proc. Combust. Inst.* **2011**, *33*, 3367−3374.
(14) Sabourin, J.; Yetter, R.; Parimi, V. S. *J. Propul. Power* **2010**, *26*, 1006−1015.
(15) Sabourin, J. L.; et al. *Propellants, Explos., Pyrotech.* **2009**, *34*, 385−393.
(16) Tyagi, H.; et al. *Nano Lett.* **2008**, *8*, 1410−1416.
(17) Van Devener, B.; Anderson, S. L. *Energy Fuels* **2006**, *20*, 1886−1894.
(18) Van Devener, B.; et al. *Energy Fuels* **2009**, *23*, 6111−6120.
(19) Sabourin, J. L.; et al. *ACS Nano* **2009**, *3*, 3945−3954.
(20) Finigan, D. J.; et al. *Combust. Flame* **2012**, *159*, 1314−1320.
(21) Ohkura, Y.; Rao, P. M.; Zheng, X. *Combust. Flame* **2011**, *158*, 2544−2548.
(22) Siegel, R.; Howell, J. R. *Thermal Radiation Heat Transfer*; Taylor and Francis: New York, 2002.
(23) Heywood, J. B. *Internal Combustion Engine Fundamentals*; McGraw-Hill: New York, 1988.
(24) Gan, Y.; Qiao, L. *Int. J. Heat Mass Transfer* **2012**, in press (http://dx.doi.org/10.1016/j.ijheatmasstransfer.2012.05.074).
(25) Jorio, A.; Dresselhaus, G.; Dresselhaus, M. S. *Carbon Nanotubes: Advanced Topics in the Synthesis, Structure, Properties and Applications*; Springer: New York, 2008.
(26) Dresselhaus, M. S.; Dresselhaus, G.; Avouris, P. *Carbon Nanotubes: Synthesis, Structure, Properties, and Applications*; Springer: New York, 2001.
(27) Berber, S.; Kwon, Y.-K.; Tománek, D. *Phys. Rev. Lett.* **2000**, *84*, 4613−4616.
(28) Che, J.; Çagin, T.; Goddard, W. A., III *Nanotechnology* **2000**, *11*, 65−69.
(29) Liu, M. S.; et al. *Int. Commun. Heat Mass Transfer* **2005**, *32*, 1202−1210.
(30) Xue, Q. *Phys. Lett. A* **2003**, *307*, 313−317.
(31) Xie, H.; et al. *J. Appl. Phys.* **2003**, *94*, 4967−4971.
(32) Liu, C. H.; et al. *Appl. Phys. Lett.* **2004**, *84*, 4248−4250.
(33) Choi, S. U. S.; et al. *Appl. Phys. Lett.* **2001**, *79*, 2252−2254.
(34) Gan, Y.; Qiao, L. *Combust. Flame* **2011**, *158*, 354−368.
(35) Gan, Y.; Qiao, L. *Int. J. Heat Mass Transfer* **2011**, *54*, 4913−4922.
(36) Modest, M. F. *Radiative Heat Transfer*; Academic Press: New York, 2003.
(37) Mishra, S. R.; et al. *Chem. Phys. Lett.* **2000**, *317*, 510−514.
(38) Sun, X.; et al. *Appl. Phys. Lett.* **1998**, *73*, 3632−3634.
(39) O'Flaherty, S. M.; et al. *J. Opt. Soc. Am. B* **2003**, *20*, 49−58.
(40) Sun, X.; et al. *Appl. Opt.* **2000**, *39*, 1998−2001.
(41) Bond, T. C.; Bergstrom, R. W. *Aerosol Sci. Technol.* **2006**, *40*, 27−67.
(42) Taylor, R. Ph.D. Dissertation, Arizona State University, Phoenix, AZ, 2011.
(43) Tien, C. L. *J. Heat Transfer* **1988**, *110*, 1230−1242.
(44) Palik, E. D. *Handbook of Optical Constants of Solids*; Elsevier Science and Technology: Amsterdam, The Netherlands, 1997.
(45) Bohren, C. F.; Huffman, D. R. *Absorption and Scattering of Light by Small Particles*; Wiley-VCH Verlag GmbH and Co. KGaA: Weinheim, Germany, 2007.